

Downward two-phase (Gas - Solid) turbulent flow through a vertical sudden expansion duct with a backward-facing step

A. S. Dawood^{1*}, A. S. Amer¹, R. M. Abumandour¹, W. A. El-Askary^{2,3}

1 Basic Engineering Science Department, Faculty of Engineering, Menoufia University, Egypt

2 Department of Mechanical Power Engineering, Faculty of Engineering, Menoufia University, Egypt

*3 Alexandria Higher Institute of Engineering & Technology (AIET), Alexandria, EGYPT
(Corresponding author: ahmed.dawood2012@sh-eng.menoufia.edu.eg)*

ABSTRACT

This study aims to investigate the impact of particles on flow characteristics within the framework of downward turbulent gas-solid flow through a sudden expansion backward-facing step. Employing the Eulerian-Lagrangian approach, the simulation encompasses both gas and solid phases. A custom FORTRAN code, based on the finite volume technique with a hybrid scheme in a staggered grid, is developed to simulate the scenario. This research introduces and compares the standard $k-\varepsilon$ and Chen-Kim turbulence models with experimental outcomes. The investigation utilizes experimental measurements and numerical simulations to comprehend flow dynamics. Upon juxtaposing the results with published experimental data, the current code displays favorable outcomes, motivating further theoretical exploration and parameter investigation. The sudden expansion backward-facing's performance is evaluated across mass loading ratios. Computational findings emphasize the considerable influence of mass loading ratio on flow behavior. An increase in mass loading ratio leads to heightened solid phase concentration and distinct flow patterns.

Keywords: Multiphase, Standard K-e model, Eulerian-Lagrangian approach.

1. Introduction

In the realm of fluid dynamics, the study of turbulent flows through complex geometries plays a pivotal role in understanding various natural and industrial processes. Among these, the phenomenon of turbulent two-phase flows through sudden expansions within backward facing step configurations holds significant importance due to its relevance in numerous practical applications. These flows are prevalent in technological domains encompassing industrial setups, energy conversion processes, and geophysical scenarios. Sudden expansions, which induce significant changes in flow parameters such as velocity and pressure, are encountered in a variety of engineering scenarios, including combustion chambers, exhaust systems, and industrial processes involving particulate-laden flows. As a result, comprehending and forecasting the turbulent traits of flows containing particles holds considerable importance as a research focus within the realm of applied fluid mechanics. Conventional computational methodologies typically rely on the utilization of the Reynolds-averaged Navier-Stokes (RANS) equations, which involve the characterization of the turbulent

spectrum through semi-empirical turbulence models. In this context, numerical simulation techniques offer an avenue for in-depth exploration. The standard $k-\varepsilon$ turbulence model, a widely employed approach in computational fluid dynamics (CFD), provides a framework for predicting the behavior of turbulent flows. By coupling this model with a focus on multiphase interactions, the current research aims to unravel the intricacies of turbulent two-phase flows through a sudden expansion within a backward facing step configuration.

Lin et al. reviewed Backward-Facing Step (BFS) flow mechanisms, extending it to model generalizations, system design implications, including heat transfer effects, and discussed control designs [1]. Ruck and Makiola experimentally studied particle dispersion in single-sided backward-facing step flow [2]. Particle size increase caused greater deviation between particle and continuous phase velocity fields. Lee and Mateescu presented experimental and numerical results for air flows over 2D backward-facing steps at various flow regimes and expansion ratios [3]. Fessler and Eaton conducted an experimental investigation of

two-phase flow within a sudden expansion and backward-facing step configuration. [4] Mean and root mean square particle velocity profiles were measured, though limited particle presence downstream of the step led to data gaps near the wall.

DNS simulation was used by Barri et al. to explore channel flow over a backward-facing step, matching upstream results with developed channel flow traits [5]. Downstream findings aligned well with experiments. Similarly, Moin and Kim used DNS for turbulent flow over a backward-facing step, revealing strong statistical agreement with experimental data [6]. Several Large Eddy Simulation (LES) investigations offer insights into particle-laden turbulent flows over backward-facing steps. YU et al. tracks particle trajectories using a particle track model, revealing intricate flow field evolution for both phases [7]. Another study by Wang et al., employs LES with a Lagrangian approach for the particle phase [8]. Additionally, Yu and Lee conducts three-dimensional numerical investigations of low-speed particle-laden flows over backward-facing steps, utilizing LES for the gas phase and Lagrangian particle tracking for the particle phase, employing a one-way coupling approach [9]. Also, Yu et al. compares 2D and 3D LES results for low and high Reynolds numbers over a backward-facing step, maintaining consistency with flow parameters and geometry [10]. These studies collectively enhance our comprehension of complex turbulent gas-particle interactions within this specific geometric configuration.

This comprehensive collection of studies aims to deepen our understanding of gas-particle flows in the context of a backward-facing step configuration. Tian et al. delves into low particle concentration gas-particle flows, evaluating predictive capabilities of the Lagrangian particle-tracking and Eulerian two-fluid models [11]. The RNG k-ε and realizable k-ε models emerge as effective turbulence models within this context. Shang focuses on gas-solid two-phase turbulent flow behind a vertical backward-facing step, comparing numerical predictions and experimental data for solid particle transport velocities [12]. A study by Benavides and Wachem, explores turbulent gas-particle flow within a vertically oriented backward-facing step, underlining the importance of accurately addressing turbulence to predict dispersed phase behavior. [13]. Riella et al. implements a Reynolds-Averaged Two-Fluid model in OpenFOAM, successfully predicting mean flow statistics for a backward-facing step [14]. Jin et al. employs the LES/FDF model for a similar study, revealing the enhanced precision of this model in gas-particle two-phase simulations [15]. Finally, Zhang et al.

introduces an anisotropic PDF model for simulating two-phase flow across a backward-facing step, using the standard $k - \epsilon$ model for gas flow and Finite Analytic/Monte Carlo Method for the PDF model, offering improved predictive potential [16]. Collectively, these studies contribute to refining our comprehension of complex gas-particle interactions in backward-facing step configurations.

2. Configuration of simulation

Fig. 1 illustrates the schematic layout of the experimental test section conducted by Fessler and Eaton [4]. The air flow's Reynolds number across the backward-facing step is calculated at 18,400, based on the maximum inlet velocity of $U_o = 10.5 \text{ m/s}$ and step height $H = 26.7 \text{ mm}$. The introduced particles within the flow are glass spheres with a diameter of $D_p = 150 \mu\text{m}$ and a density of $\rho_p = 2500 \text{ kg/m}^3$. The numerical simulation is conducted utilizing identical flow parameters and geometric configurations as those employed in the experimental study.

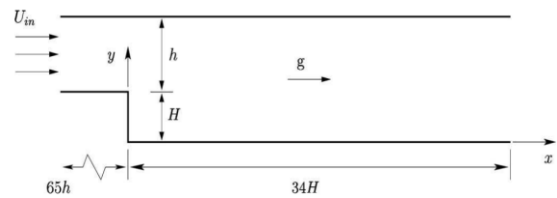


Fig. 1 Schematic diagram of the test section.

3. Mathematical model

The Eulerian-Lagrangian technique is used to study two phase (particle laden) flow. Eulerian equations are used to simulate continuous phases, while Lagrangian equations' trajectory technique is used to anticipate solid particles.

3.1 Continuous phase model (Gas phase)

For a general, Newtonian incompressible, isothermal, turbulent, axisymmetric (no angular changes), steady-state flow, the motion of gas is given by the continuity equation with Reynolds averaged Navier stokes equations (RANS) in cartesian coordinates. This is how the governing equation is expressed according to Fig. 1:

$$\frac{\partial}{\partial x}(\rho u \varphi) + \frac{\partial}{\partial y}(\rho v \varphi) = \frac{\partial}{\partial x} \left(\Gamma_{\varphi} \frac{\partial \varphi}{\partial x} \right) + \frac{\partial}{\partial y} \left(\Gamma_{\varphi} \frac{\partial \varphi}{\partial y} \right) + S_{\varphi} \tag{1}$$

where φ is the generalized dependent variable, Γ_{φ} is the transport coefficient, S_{φ} is the source term of the continuous phase, and S_p^{φ} is the source term due to fluid-particles interaction. Each variable's definition for the governing equation is provided in Table (1).

Table 1 Variables included in the governing equations for the gas phase.

Conservation of	φ	Γ_φ	S_φ
Continuity	1	0	0
x-Momentum	u	μ_{eff}	$-\frac{\partial p}{\partial x} + \frac{\partial}{\partial x}(\mu_{eff} \frac{\partial u}{\partial x}) + \frac{\partial}{\partial y}(\mu_{eff} \frac{\partial v}{\partial x})$
y-Momentum	v	μ_{eff}	$-\frac{\partial p}{\partial y} + \frac{\partial}{\partial x}(\mu_{eff} \frac{\partial u}{\partial y}) + \frac{\partial}{\partial y}(\mu_{eff} \frac{\partial v}{\partial y})$
Turbulent kinetic energy	k	$\frac{\mu_{eff}}{\sigma_k}$	$(G_k - C_D \rho \varepsilon)$
Dissipation rate of turbulent kinetic energy	ε	$\frac{\mu_{eff}}{\sigma_\varepsilon}$	$\frac{\varepsilon}{k} (c_{\varepsilon 1} G_k - c_{\varepsilon 2} \rho \varepsilon + \frac{c_{\varepsilon 3} G_k^2}{\rho \varepsilon})$

where G_k is the generation term of the turbulent kinetic energy, ε is the turbulent dissipation rate, μ_{eff} is the effective viscosity, and ρ is the continuous phase density. The generation term is given as follows:

$$G_k = \mu_t \left[2 \left(\left(\frac{\partial u}{\partial x} \right)^2 + \left(\frac{\partial v}{\partial y} \right)^2 \right) + \left(\frac{\partial u}{\partial y} + \frac{\partial v}{\partial x} \right)^2 \right] \quad (2)$$

$$\mu_{eff} = \mu + \mu_t \quad (3)$$

where μ_t is the turbulent viscosity and can be modeled for the k- ε turbulence models as:

$$\mu_t = \rho C_\mu \frac{k^2}{\varepsilon} \quad (4)$$

and S_p^u, S_p^v are the particle momentum source terms in axial and wall normal directions, respectively, while S_p^k, S_p^ε are the particle turbulence source terms.

In the present study, the standard $k - \varepsilon$ and Chen kim models are used and the turbulence constants of these model are summarized in table (2) as given by Hamed [17].

Table 2 The turbulence models constants.

Turbulence model	$C_{\varepsilon 1}$	$C_{\varepsilon 2}$	$C_{\varepsilon 3}$	C_D	C_μ	σ_k	σ_ε
Standard $k - \varepsilon$	1.44	1.92	0.0	1.0	0.09	1.0	1.3
Standard Chen-kim	1.15	1.9	0.25	1.0	0.09	0.75	1.15

3.2 Solid Phase Model

When the spherical solid particles collide with the wall and one another, it is assumed that they remain rigid bodies (undeformed). The channel with pressure gradients is traced using a Lagrangian technique with a finite number of parcels and a finite number of particles with a diameter D_p in each parcel. The particle tracking method is used in which a system of ordinary differential equations is used to predict the translational and angular velocities u_p, v_p and ω_p respectively along the particle path. This system of O.D.E as in El-Behery et al. [18] is solved using 4th order Runge-kutta method.

$$m_p \frac{d\vec{u}_p}{dt} = \vec{F}_G + \vec{F}_D + \vec{F}_{SL} + \vec{F}_{ML} \quad (5)$$

$$\frac{d\vec{z}_p}{dt} = \vec{V}_p \quad (6)$$

$$\vec{T} = \pi \mu d_p^3 (0.5 \nabla \times \vec{V}_f - \vec{\omega}_p) \quad (7)$$

$$\vec{T} = I_p \frac{d\vec{\omega}_p}{dt} \quad (8)$$

where $\vec{F}_G, \vec{F}_D, \vec{F}_{SL}, \vec{F}_{ML}$ are the gravity, drag, Saffman lift, and Magnus lift forces, respectively, \vec{V}_f and \vec{V}_p are the fluid and particle velocity vectors respectively, \vec{z}_p is the particle position vector, $\vec{\omega}_p$ is the particle angular velocity vector, m_p is the mass of the particle, while \vec{T} is the torque acting on the particle due to fluid rotation.

Assuming spherical particles, the moment of inertia for the spherical bodies I_p is given by:

$$I_p = 0.1 m_p d_p^2 \quad (9)$$

3.2.1. The gravity force

This force, which originates from the disparity between fluid weight and particle weight, is represented by the following expression:

$$\vec{F}_G = m_p \vec{g} \left(\frac{\rho}{\rho_p} - 1 \right) \quad (10)$$

3.2.2. The drag force

This is the resistance force brought on by a body moving in a flow field, and it may be calculated using the equation below:

$$\vec{F}_D = \frac{3}{4} \frac{\rho m_p}{\rho_p d_p} C_D (\vec{V}_f - \vec{V}_p) |\vec{V}_f - \vec{V}_p| \quad (11)$$

Where ρ_p is the particle density and C_D is the drag coefficient and can be expressed as a function of particle-Reynolds number as in Hamed [17]:

$$Re_p = \frac{\rho d_p |\vec{u} - \vec{u}_p|}{\mu} \quad (12)$$

$$C_D = \left\{ \begin{array}{ll} \frac{24}{Re_p} & Re \leq 1 \\ \frac{24}{Re_p^{0.646}} & 1 < Re \leq 400 \\ \begin{array}{ll} 0.5 & 400 < Re \leq 3 \times 10^5 \\ 0.000366 Re_p^{0.4275} & 3 \times 10^5 < Re \leq 2 \times 10^6 \\ 0.18 & Re > 2 \times 10^6 \end{array} \end{array} \right\} \quad (13)$$

3.2.3. The shear lift force

Since the relative velocities around the particle are not uniform, the shear lift results from the inertia effects in the viscous flow and is provided by the following equation as in Mei [19]:

$$\vec{F}_{SL} = 1.615 d_p^3 \rho_f Re_s^{-0.5} C_{SL} [(\vec{V}_f - \vec{V}_p) \times \vec{\omega}_f] \quad (14)$$

where C_{SL} is the shear lift coefficient representing the ratio of extended lift force to Saffman force as given in [19]:

If $Re_p \leq 40$ then,

$$C_{SL} = (1 - 0.3314 \gamma^{0.5}) e^{-0.1 Re_p} + 0.3314 \gamma^{0.5} \quad (15)$$

While, if $Re_p > 40$ then,

$$C_{SL} = 0.0524 (\gamma Re_p)^{0.5} \quad (16)$$

$$\gamma = 0.5 \frac{Re_s}{Re_p} \quad (17)$$

where $Re_s = \frac{\rho d_p^2 |\vec{\omega}_f|}{\mu}$ is the particle Reynolds number of the shear flow and $\vec{\omega}_f = 0.5(\nabla \times \vec{V}_f)$ is the fluid vorticity.

3.2.4. The Magnus lift force

The Magnus effect, which is a measurable phenomenon frequently connected to a rotating item moving in a fluid, depends on the rotational speed and is expressed as Lun and Liu [20]:

$$\vec{F}_{ML} = \frac{1}{2} \rho \vec{V}_r^2 \frac{\pi d_p^2}{4} C_{LM} \frac{\vec{\omega}_r \times \vec{V}_r}{|\vec{\omega}_r| |\vec{V}_r|} \quad (18)$$

where C_{LM} is known as Magnus lift coefficient and is calculated as:

$$C_{ML} = \frac{d_p |\vec{\omega}_r|}{|\vec{V}_r|} \quad Re_p \leq 1 \quad (19)$$

$$C_{ML} = \frac{d_p |\vec{\omega}_r|}{|\vec{V}_r|} [0.178 + 0.822 Re_p^{-0.522}] \quad Re_p \leq 10^3 \quad (20)$$

where $\vec{V}_r = (\vec{V}_f - \vec{V}_p)$ is the relative linear velocity vector and $\vec{\omega}_r = \vec{\omega}_f - \vec{\omega}_p$ is the relative angular velocity vector.

The total instantaneous fluid velocity at a specified position for the particle inside a cell is the sum of the mean fluid velocity vector \vec{V} and the fluctuating velocity vector V' at the particle position. The fluctuating velocity vector \vec{V}' is calculated by generating a random value clarifying the fluctuation as in El-Askary et al. [21]:

$$V' = \zeta \sqrt{\frac{2k}{3}} \quad (21)$$

where ζ is a random number with zero mean and unity variance, and k is the turbulent kinetic energy at the particle position in the cell. Then the total instantaneous fluid velocity is given by El-Askary et al. [21]:

$$\vec{V}_f = \vec{V} + \vec{V}' \quad (22)$$

Calculating the instantaneous fluid velocity at the particle position is needed during the solid phase solution where the fluid velocity, the relative linear velocity, and relative angular velocity are required into equations (11) to (20).

The time step used in equations (5), (6) and (8) which are solved by 4th order Runge Kutta method is known as Lagrangian time step Δt_L . As in El-Askary et al. [21] and Shuen et al. [22], this time step should be less than or equal the interaction time between the generated eddy and the particle. The interaction time is the minimum time between two times (time required for the particle to pass the eddy τ_{tr} & eddy life time τ_e). ($\tau_{int} = \min(\tau_e, \tau_{tr})$)

where $\tau_{tr} = -\tau_p \ln(1 - \frac{l_e}{\tau_p |\vec{u} - \vec{u}_p|})$ is the transverse time, $\tau_p = \frac{d_p^2 \rho_p}{18\mu}$ is the particle time, $\tau_e = \frac{l_e}{\sqrt{\frac{2k}{3}}}$ is the

eddy life time, and $l_e = \frac{C_\mu^{3/4} k^{3/2}}{\varepsilon}$ is the dissipation length scale.

3.3 Particle Wall Collision

Because the particles in this study are rigid, and spherical, there is no deformation caused by collisions, and the particle material properties are the same. The two types of impact that can occur between a moving object and a stationary wall are adhesive and sliding impact. When there is an adhesive impact, the particle stops sliding on the wall during the impact time, however, when there is a sliding impact, the particle keeps sliding. After a collision, the particle's velocities alter concerning the wall's static and dynamic friction

coefficients, as well as the particle's restitution coefficient with the solid surface.

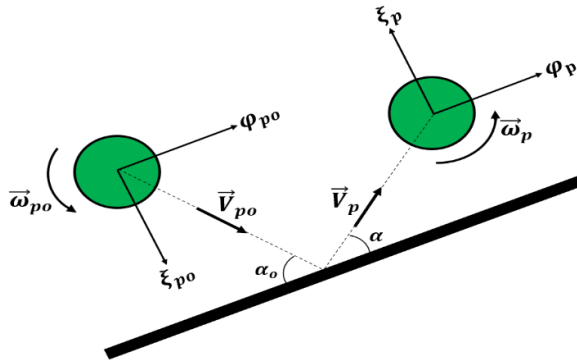


Fig. 2 Particle–wall collision.

The equations that describe the particle motion (linear and angular velocities) after the particle-wall collision are given by Sommerfeld and Huber [23], Heinel and Bohnet [24] and can be written as a general model where φ_{p0} , ξ_{p0} , are the parallel and normal components of the particle velocity before collision, and ω_{p0} is the particle angular velocity before collision while, φ_p , ξ_p , ω_p are the parallel, normal and angular particle velocities after collision as shown in Fig. 2.

In the adhesive impact, the following equation must be achieved:

$$\varphi_{p0} + \frac{D_p \omega_{p0}}{2} \leq \frac{7}{2} \mu_s (1 + e) |\xi_{p0}| \quad (23)$$

where μ_s is the static friction coefficient, e is the restitution coefficient.

In this study as Sommerfeld [25], the values of static and restitution coefficients are $\mu_s = 0.4$, $e = 0.9$

If Eq. (23) is met, the linear and angular velocity components after impact can be written as:

$$\varphi_p = \frac{5}{7} (\varphi_{p0} - \frac{D_p}{5} \omega_{p0}) \quad (24)$$

$$\xi_p = -e \xi_{p0} \quad (25)$$

$$\omega_p = -\frac{2\varphi_p}{D_p} \quad (26)$$

If Eq. (23) is not satisfied, the impact type is a sliding impact and the rebound linear velocities and angular velocity of the particle after impact are given by:

$$\xi_p = -e_w \xi_{p0} \quad (27)$$

$$\varphi_p = \varphi_{p0} - \mu_d (1 + e) \varepsilon_o \xi_{p0} \quad (28)$$

$$\omega_p = \omega_{p0} + \frac{5\mu_d(1+e)\varepsilon_o \xi_{p0}}{D_p} \quad (29)$$

where μ_d is the dynamic friction coefficient ($\mu_d = 0.15$), and ε_o indicates the direction of relative velocity between the particle surface and the wall and is given by:

$$\varepsilon_o = \text{sign}(\varphi_{p0} - \frac{D_p}{2} \omega_{p0}) \quad (30)$$

3.4 Particle-Particle Collision

It is taken into account how particle-particle collisions can affect the linear and rotational velocities of the colliding particles. As illustrated in Fig. 3, the model is simulated in the current work utilizing a stochastic technique with virtual (subscripted by 1) and actual (subscripted by 2) moving particles. The actual particle is the moving particle in the current iteration with updated properties such as linear and rotational velocities, whereas the virtual particle has properties that are identical to the average value of properties in the domain cell in the previous iteration of the solution. Because particle-particle collision is a random process, it is simulated using a probability function, which is provided by Oesterle and Petitjean [26]:

$$P_c = 1 - e^{-N_{p1} \Delta t_L (D_{p1} + D_{p2}) |\vec{V}_{p2} - \vec{V}_{p1}|} \quad (31)$$

where N_{p1} is the number of particles per unit time in the computational cell computed from the previous iteration, Δt_L is the Lagrangian time step, D_{p1} and D_{p2} are the virtual and actual particles diameters, in this study ($D_{p1} = D_{p2}$), \vec{V}_{p1} and \vec{V}_{p2} are the velocity vectors of virtual and actual moving particle.

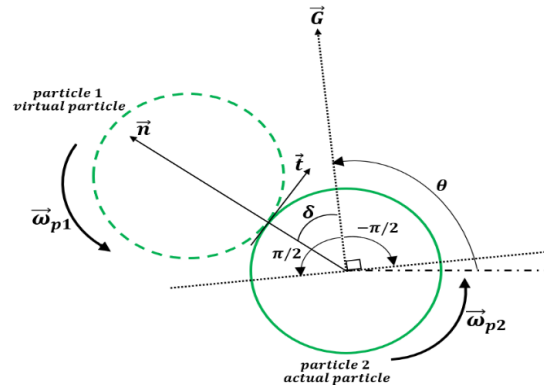


Fig. 3 Particle–particle collision.

The virtual and actual moving particles collide if the probability function described in Eq. (31) is greater than a randomly generated value produced from a dispersed interval [0,1]. Another random value arises (Random collision angle) which determines the location where the collision takes place. This angle is ($\delta \in [-\pi/2, \pi/2]$) as in Fig. 2.

The particle-particle collision can occur in sliding or non-sliding collisions, just like the particle-wall collision. The following relation must hold for the sliding collision to occur as mentioned in Crowe et al. [27]:

$$\frac{\vec{n} \cdot \vec{G}^{(0)}}{|\vec{G}_{ct}^{(0)}|} < \frac{2}{7} \cdot \frac{1}{f_p (1 + e_p)} \quad (32)$$

where \vec{n} is the unit normal vector, $\vec{G}^{(0)}$ is the relative velocity before impact and $\vec{G}_{ct}^{(0)}$ is the tangential

relative velocity component before collision at the contact point and they can be derived according to Fig. 2 as:

$$\vec{n} = (\cos \gamma)\vec{i} + (\sin \gamma)\vec{j} \quad (33)$$

$$\gamma = \theta + \delta \quad (34)$$

$$\vec{G}^{(0)} = (u_{p1}^{(0)} - u_{p2}^{(0)})\vec{i} + (v_{p1}^{(0)} - v_{p2}^{(0)})\vec{j} \quad (35)$$

$$\vec{G}_{ct}^{(0)} = \vec{G}^{(0)} - (\vec{n} \cdot \vec{G}^{(0)})\vec{n} + 0.5D_{p1}\vec{\omega}_{p1}^{(0)} \times \vec{n} + 0.5D_{p2}\vec{\omega}_{p2}^{(0)} \times \vec{n} \quad (36)$$

$$\vec{t} = \frac{\vec{G}_{ct}^{(0)}}{|\vec{G}_{ct}^{(0)}|} \quad (37)$$

where \vec{t} denotes the tangential unit vector, subscript (o) refers to the condition before impact and f_p, e_p are the friction and restitution coefficients ($f_p = 0.4, e_p = 0.95$).

If Eq. (32) is valid, a sliding collision occurs, and the particle's post-collision linear and angular velocities are given by Sommerfeld [25]:

$$\vec{V}_{p2} = \vec{V}_{p2}^{(0)} - (\vec{n} - f_p\vec{t})(\vec{n} \cdot \vec{G}^{(0)})(1 + e_p)\frac{m_{p1}}{m_{p1}+m_{p2}} \quad (38)$$

$$\vec{\omega}_{p2} = \vec{\omega}_{p2}^{(0)} + \left(\frac{5}{D_{p2}}\right)(\vec{n} \cdot \vec{G}^{(0)})(\vec{n} \times \vec{t})f_p(1 + e_p)\frac{m_{p1}}{m_{p1}+m_{p2}} \quad (39)$$

If the particle stops sliding after collision, the collision is a non-sliding collision, and the after collision velocities are:

$$\vec{V}_{p2} = \vec{V}_{p2}^{(0)} - \left\{(\vec{n} \cdot \vec{G}^{(0)})(1 + e_p)\vec{n} + \left(\frac{2}{7}\right)|\vec{G}_{ct}^{(0)}|\vec{t}\right\}\frac{m_{p1}}{m_{p1}+m_{p2}} \quad (40)$$

$$\vec{\omega}_{p2} = \vec{\omega}_{p2}^{(0)} - \left(\frac{10}{7D_{p2}}\right)|\vec{G}_{ct}^{(0)}|(\vec{n} \times \vec{t})\frac{m_{p1}}{m_{p1}+m_{p2}} \quad (41)$$

where m_{p1} and m_{p2} are the masses of the virtual and actual particles, respectively.

3.5 Coupling between the two phases

The source terms $S_p^u, S_p^v, S_p^k,$ and S_p^ε stated in the gas phase equations serve as the links between the two phases and are taken into account in the current study when coupling momentum between gas and solid is involved. The inclusion of solid particles in the computational cell also results in a decrease in gas volume. The term $\overline{S_p^V}$ that links two phases is given by Lun and Liu [20]:

$$\overline{S_p^V} = \frac{\beta\rho_p}{m_p N_p} \sum_{i=1}^{N_t} \vec{F} \quad (42)$$

where N_p is the number of particles per unit time in the computational cell, N_t is the total number of trajectories, m_p is the mass of the solid particle, ρ_p is the particle density, \vec{F} is the sum of all forces acting on the particle and β is the volume void fraction that the particle occupies (The sum of $\frac{N_p\Delta t_L V_p}{V_c}$ over all

trajectories that pass through the computational cell) and can be calculated using the trajectory method as in El-Askary et al [21], and Crowe et al. [27]:

$$\beta = \sum_{traaj} \frac{N_p\Delta t_L V_p}{V_c} \quad (43)$$

where Δt_L is the lagrangian time step, V_p is the volume of one particle and V_c is the volume of the computational cell.

Since the volume of the entire cell is unity, the gas void fraction is equal to the difference between the volume of the cell and the volume that its particles occupy, and it may be computed as follows:

$$\alpha_g = 1 - \beta \quad (44)$$

The turbulent kinetic energy and dissipation rate source terms can be expressed as Eghlimi et al. [28]:

$$\overline{S_p^k} = 2k\frac{\beta\rho_p}{\tau_p}\left(1 - e^{-\beta k\frac{\tau_p}{\tau_l}}\right) \quad (45)$$

$$\overline{S_p^\varepsilon} = 2\varepsilon\frac{\beta\rho_p}{\tau_p}\left(1 - e^{-\beta\varepsilon\frac{\tau_p}{\tau_l}}\right) \quad (46)$$

where $\tau_l = \frac{k}{\varepsilon}$ and $\beta_k, \beta_\varepsilon$ are constants and equal 0.09, 0.4 respectively.

4. Boundary conditions

For the inlet condition, the particle velocity is assumed to be constant, depending on the particle mass flow rate, while the turbulent kinetic energy and its dissipation rate are assumed to be constant. The gas flow velocity is assumed to follow a 1/7th power-law profile. The wall-function approximation is employed to assume no-slip boundary conditions for solid walls referring to El-Askary and Balabel [29]. At the centerline, the symmetric boundary conditions are applied to all variables. The axial gas velocity is corrected at the exit to satisfy the mass balance.

5. Solution Strategy

To solve the governing equations for pressure-velocity coupling in a steady flow utilizing a staggered grid and the SIMPLE algorithm, a finite volume discretization with a hybrid differencing scheme technique is presented. The Tri-diagonal Matrix Algorithm is used to solve the discretized equations. The 4th-order Runge-Kutta technique with the Lagrangian time step is used to solve the ordinary differential equations that describe particle motion, and the solution process is broken down into the following steps as in [30]:

- 1- Firstly, the domain is discretized and has an initial value for all variables.
- 2- Solution of gas phase is obtained until convergence, (maximum normalized residuals

- 0.0005), considering no source terms and no solid void fraction with unity gas void fraction.
- 3- Parcels are traced at the pipe inlet with the entry conditions mentioned above.
 - 4- The solution of the solid phase is obtained with a small time step considering all effects on the solid phase such as dispersion, all forces, and particle-wall collisions.
 - 5- The particle-particle collisions are not considered in the first iteration only where there is no old data for the solid phase such as velocities and number of parcels.
 - 6- Tracking all the trajectories that pass each computational cell, solid and gas void fractions, momentum, and turbulence source terms are computed and stored.
 - 7- The particle properties are stored as virtual data for the next iteration where used in the particle-particle collisions and the solution continues until the last parcel.
 - 8- The solution of the gas phase is resolved taking into consideration the gas void fractions and source terms computed in step 6.
 - 9- Repeat steps from 2 to 8 till overall convergence in all variables.

6. Results and discussion

6.1 Velocity profiles of the gas phase

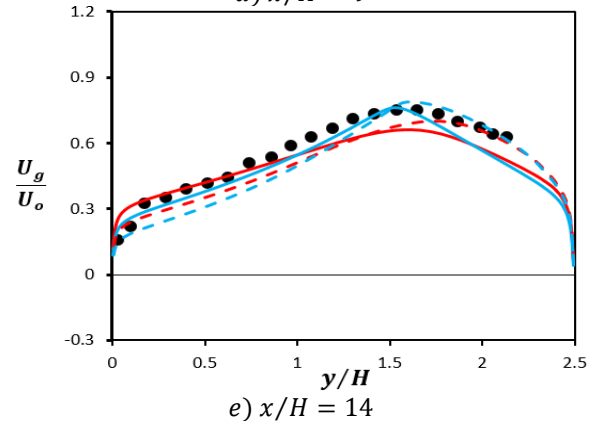
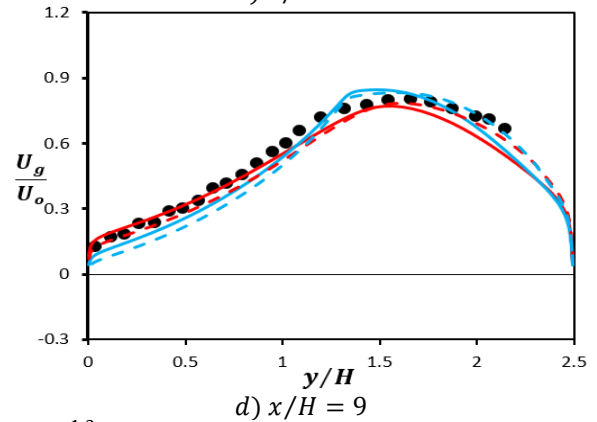
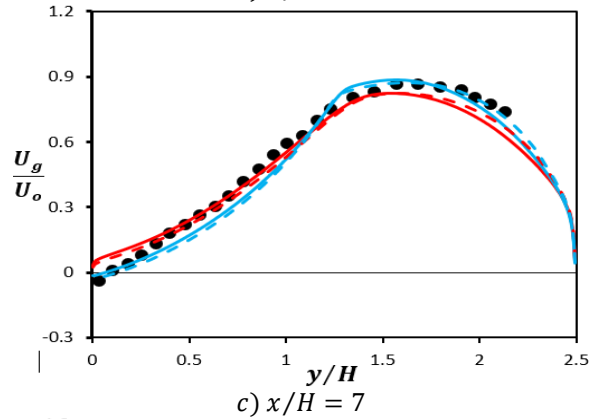
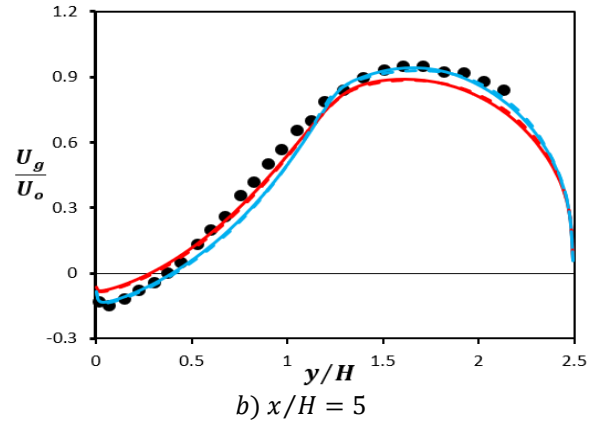
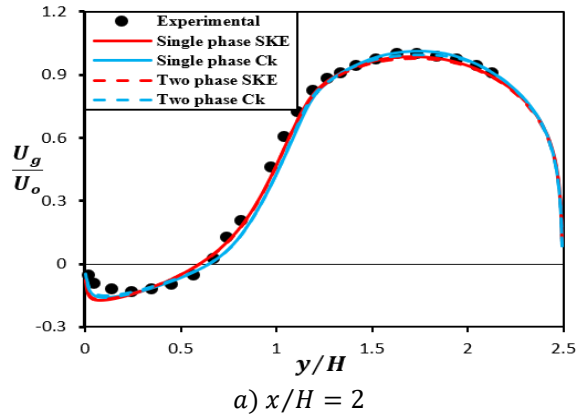


Fig. 4 Streamwise mean velocity (gas phase).

Fig. 4 illustrates the predicted streamwise mean velocity profiles of the gas phases at varying downstream positions ($x/H = 2, 5, 7, 9,$ and 14), alongside corresponding experimental data [4]. The simulation showcases substantial agreement with the experimental results [4]. As noted in [4], particle presence was notably absent in the separation zone behind the step at positions ($x/H = 2$ and 5). Minimal discrepancies are observed between the SKE and Ck turbulence models across positions ($x/H = 2, 5, 7,$ and 9). Generally, the Chen-kim model demonstrates improved flow prediction near the duct's centerline region, while the SKE model performs better near the straight wall region.

The streamlines of the gas phase in the presence of the $150 \mu\text{m}$ diameter glass particles is shown in Fig. 5. A recirculation zone behind the step wall is formed due to the strong adverse pressure gradient. The predicted reattachment length of ($x = 0.198, x/H = 7.416$) agrees well with the experimental results of [4]. In the LES simulation study [7], there was a secondary circulation zone at ($x/H = 2.38$) and it was not predicted in the experimental work [4] and also using Reynolds averaged equations in Ref. [31].

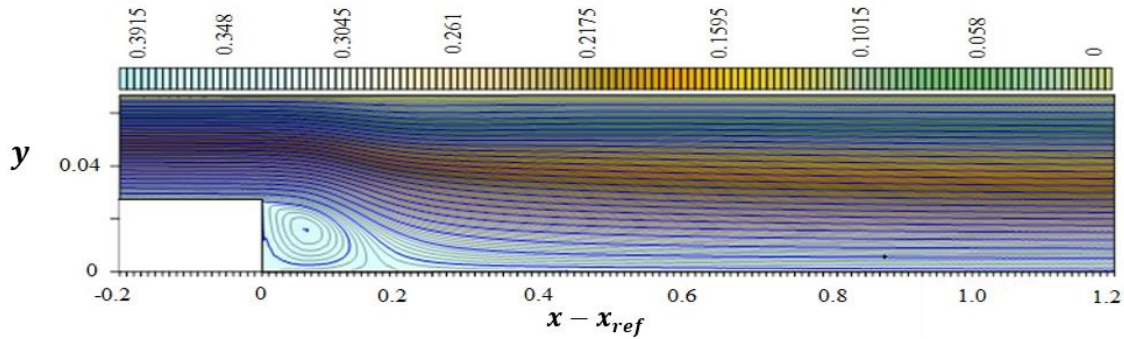
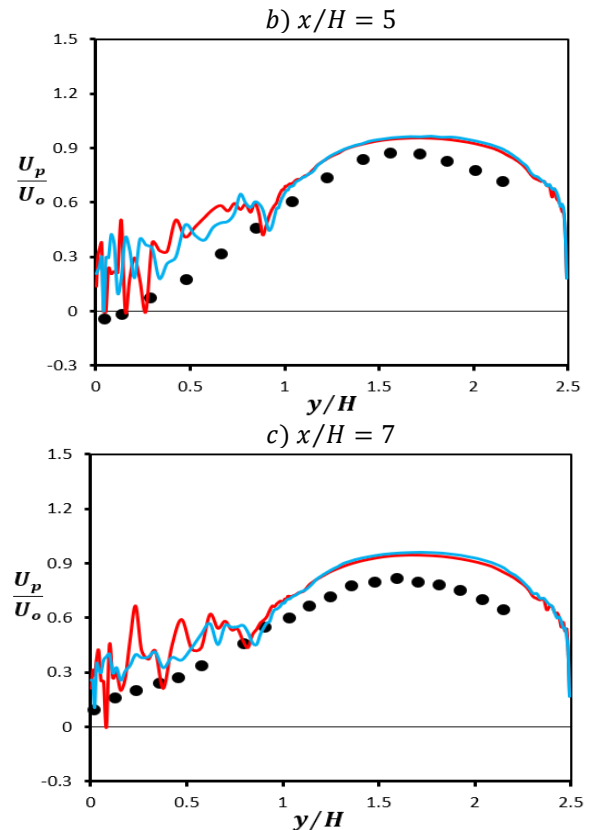
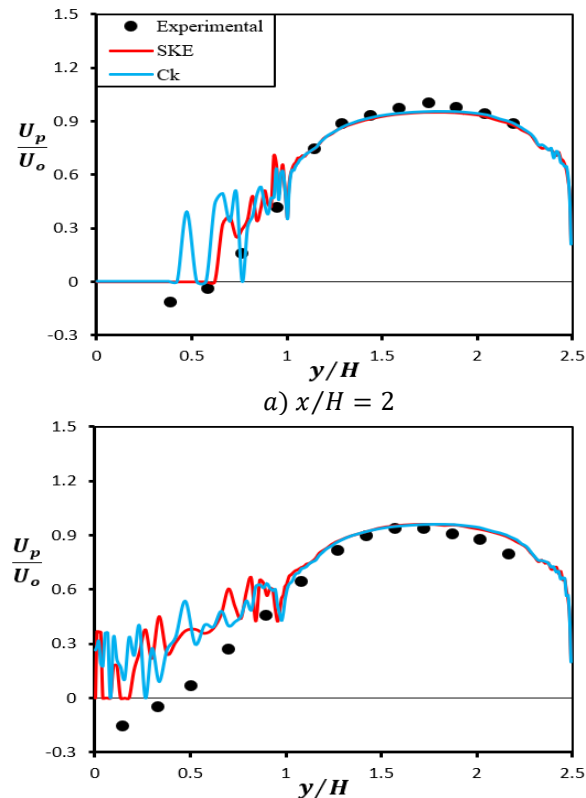


Fig. 5 Mean streamwise flow pattern (gas phase).

6.2 Axial velocity profiles of the solid phase



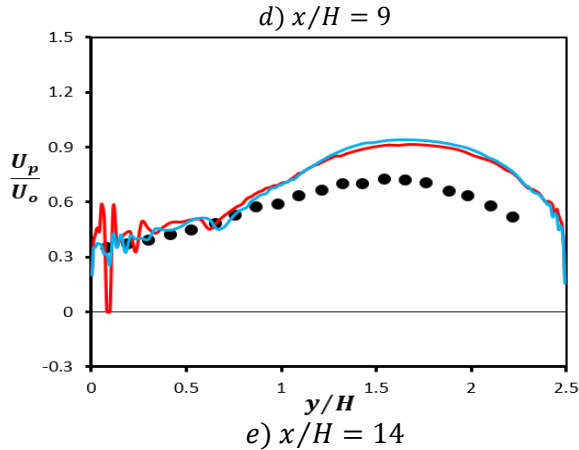


Fig. 6 Streamwise mean velocity profiles for the 150 μm glass particles.

Validation of the glass particles' mean axial velocities is shown in Fig. 6. The inlet velocity of the particle is 3 % of the gas inlet velocity. The model predicts well the flow near the straight wall of the duct and poorly expects the velocities near the recirculation zone at ($x/H = 2$ and 5). The SKE and Ck models predicts the results similarly and well with the experimental data of [4].

6.3 Pressure recovery coefficient along the sudden expansion wall

In fluid dynamics, particularly when studying flow through abrupt changes in geometry like a backward-facing step, the pressure of the fluid can change significantly due to alterations in velocity, turbulence, and other flow characteristics. According to the air density ρ and inflow velocity U_{in} , the pressure coefficient C_p has been dimensionalized as follows:

$$C_p = \frac{(P_x - P_{x=0})}{0.5 \rho U_{in}^2} \quad (47)$$

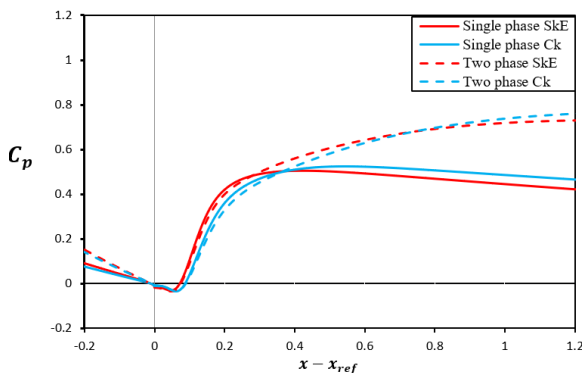


Fig. 7 Pressure recovery Coefficient along the sudden expansion wall.

Fig. 7 shows the pressure recovery coefficient along the sudden expansion wall in the single and two phase.

Due to the cross sectional area increases due to the expansion, the pressure drop increases as the gas velocity decreases according to Bernoulli's equation. When particles are introduced into the flow, they can significantly alter the flow behavior, leading to changes in pressure distribution. The interactions between particles and the fluid can affect the momentum exchange, turbulence, and energy dissipation within the flow field leading to an increase in the pressure recovery.

6.4 Skin friction coefficient along the sudden expansion wall

In fluid dynamics, the skin friction coefficient (C_f) is a dimensionless parameter used to characterize the frictional drag force exerted by the fluid on a surface. It is a crucial parameter in assessing the flow resistance and energy losses within a fluid system. The measured skin friction coefficient is calculated as:

$$C_f = \frac{\tau_{wall}}{0.5 \rho U_{in}^2} \quad (48)$$

where τ_{wall} is the wall shear stress.

Fig 8. Reveals the skin friction coefficient along the sudden expansion wall in the single phase and in the presence of the solid particles. When particles are introduced into a flow, they can disrupt the smooth flow of the fluid near the surface, leading to increased frictional resistance and potentially higher skin friction coefficients.

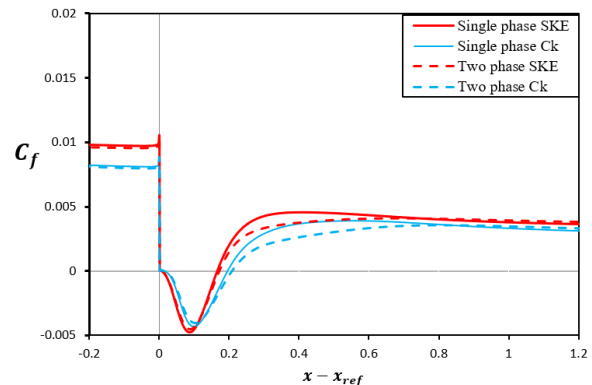


Fig. 8 Skin friction Coefficient along the sudden expansion wall.

6.5 Effect of mass loading ratio

The effect of the mass loading ratio on the pressure coefficient shown in Fig. 9, refers to how changes in the concentration of solid particles relative to the fluid phase impact the pressure distribution along the flow path. When the mass loading ratio increases (from 0.5 to 1.5), meaning more solid particles are introduced into the fluid, several effects on the pressure coefficient can occur. It leads to increased momentum exchange between the fluid and particles and so

increased pressure recovery coefficient. Also, solid particles can interact with the fluid, affecting the overall flow structure. These interactions may lead to variations in the pressure coefficients.

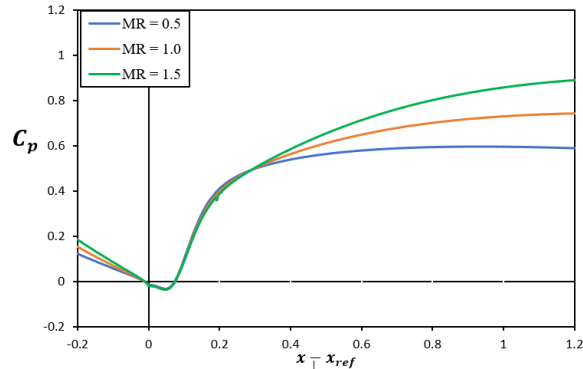


Fig. 9 Pressure recovery coefficient along the sudden expansion wall for different mass loading ratios.

It is shown from Fig. 10 the effect of mass loading ratio on the skin friction coefficient along the sudden expansion. Generally, an increase in the mass loading ratio often leads to an increase in the skin friction coefficient and it is shown after the separation zone. This is because the presence of solid particles in the fluid disrupts the smooth flow near the surface, creating additional frictional resistance. As more particles are introduced into the flow, the interactions between the particles and the fluid increase, which can result in higher shear stresses and a higher skin friction coefficient along the surface of the step geometry.

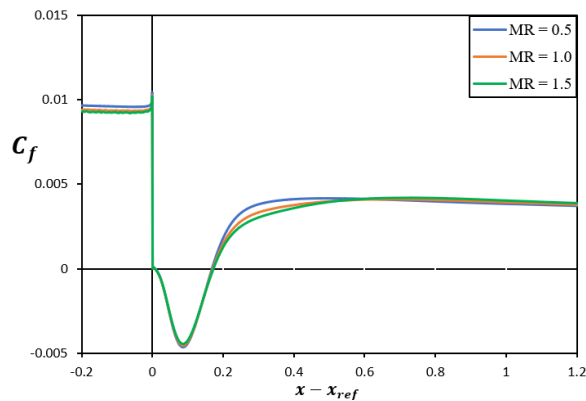


Fig. 10 Skin friction coefficient along the sudden expansion wall for different mass loading ratios.

7. Conclusion

In summary, this research focuses on investigating how particles influence flow characteristics in downward turbulent gas-solid flow through a sudden expansion backward-facing step. Utilizing the Eulerian-Lagrangian approach and a custom FORTRAN code, the study examines both gas and

solid phases, comparing standard $k - \epsilon$ and Chen-Kim turbulence models with experimental data. The developed code aligns well with experimental results through gas and particle velocity profiles, inspiring further exploration. Findings emphasize the impact of mass loading ratio and particle diameter on flow behavior, revealing heightened solid concentration with increased mass loading and significant effects of particle diameter on pressure distribution, skin friction coefficient along the wall. This work contributes valuable insights into particle-fluid interactions in complex flow scenarios and offers a foundation for future investigations.

8. References

- [1] C. Lin , A. Keisuke , N. Taku , X. Guannan and L. Tianshu , "A review of Backward-Facing Step (BFS) flow mechanisms, heat transfer and control," Thermal Science and Engineering Progress, vol. 6, pp. 194-216, 2018.
- [2] B. Ruck and B. Makiola, "Particle dispersion in a single-sided backward-facing step flow," International Journal of Multiphase Flow, vol. 14, pp. 787-800, 1988.
- [3] T. LEE and D. MATEESCU, "Experimental and numerical investigation of 2-d backward-facing step flow," Journal of Fluids and Structures, vol. 12, pp. 703-716, 1998.
- [4] J. R. Fessler and J. K. Eaton , "Turbulence modification by particles in a backward-facing step flow," Journal of Fluid Mechanics, vol. 394, pp. 97-117, 1999.
- [5] M. Barri, G. K. El Khoury, H. I. Andersson and B. Pettersen, "DNS of backward-facing step flow with fully turbulent inflow," International Journal for Numerical Methods in Fluids, vol. 64, pp. 777-792, 2010.
- [6] H. LE, P. MOIN and J. KIM, "Direct numerical simulation of turbulent flow over a backward-facing step," Journal of Fluid Mechanics, vol. 330, pp. 349-374, 1997.
- [7] K. F. YU, K. S. Lau and C. K. Chan, "Numerical simulation of gas-particle flow in a single-side backward-facing step flow," Journal of Computational and Applied Mathematics, vol. 163, pp. 319-331, 2004.
- [8] B. Wang, H.-q. Zhang, X.-l. Wang, Y.-c. Guo and W.-y. Lin , "Large eddy simulation of a particle-laden turbulent backward-facing step flow," 4th ASME_JSME Joint Fluids Engineering Conference, 2003.
- [9] K. Yu and E. W. Lee, "Evaluation and modification of gas-particle covariance models

- by Large Eddy Simulation of a particle-laden turbulent flows over a backward-facing step," *International Journal of Heat and Mass Transfer*, vol. 52, pp. 5652-5656, 2009.
- [10] K. F. Yu, E. W. M. Lee and J. K. Yuen, "High and Low Reynolds Number Two-phase Flows over a Backward-facing Step by 2D and 3D Large Eddy Simulation," *International Journal of Nonlinear Sciences and Numerical Simulation*, vol. 10, pp. 1135-1158, 2009.
- [11] . Z. F. Tian, J. Y. Tu and . G. H. Yeoh, "Numerical simulation and validation of dilute gas-particle flow over a backward-facing step," *Aerosol Science and Technology*, vol. 39(4), pp. 319-332, 2005.
- [12] Z. Shang, "CFD of turbulent transport of particles behind a backward-facing step using a new model— $k-\epsilon$ -Sp," *Applied Mathematical Modelling*, vol. 29, pp. 885-901, 2005.
- [13] A. Benavides and B. van Wachem, "Eulerian-Eulerian prediction of dilute turbulent gas-particle flow in a backward-facing step," *International Journal of Heat and Fluid Flow*, vol. 30, pp. 452-461, 2009.
- [14] M. Riella, R. Kahraman and G. Tabor, "Reynolds-Averaged Two-Fluid Model prediction of moderately dilute fluid-particle flow over a backward-facing step," *International Journal of Multiphase Flow*, vol. 106, pp. 95-108, 2018.
- [15] H. Jin , Y. Chen , J. Fan and K. Luo, "LES/FDF simulation of a gas-particle backward-facing step flow," *Chemical Engineering Science*, vol. 66, pp. 3692-3700, 2011.
- [16] P. Zhang, J. Xu and N. Ding, "Numerical Simulating for Backward Facing Step Particle Laden Flow Using Anisotropic PDF Mode," *International Conference on Computing, Control and Industrial Engineering*, Wuhan, China, 2010, vol. 2 IEEE, pp. 222-225, 2010.
- [17] M. H. Hamed, "Numerical simulation of gas-solid two-phase flow in a two dimensional horizontal channel with sudden expansion," *Alex. Eng. J.*, vol. 620 (4), pp. 435-453, (2006).
- [18] S. M. El-Behery, W. A. El-Askary, M. H. Hamed and K. A. Ibrahim, "Hydrodynamic and thermal fields analysis in gas-solid two-phase flow," *Int. J. Heat Fluid Flow*, vol. 32, pp. 740-754, (2011).
- [19] R. Mei, "An approximate expression for the shear lift force on a spherical particle at finite Reynolds number," *Int. J. Multiphase Flow*, vol. 18, pp. 145-147, (1992).
- [20] C. C. K. Lun and H. S. Liu, "Numerical simulation of dilute turbulent gas-solid flows in horizontal channels," *Int. J. Multiphase Flow*, vol. 23, p. 575-605, (1997).
- [21] W. A. El-Askary, K. A. Ibrahim, S. M. El-Behery, M. H. Hamed and M. S. Al-Agha, "Performance of vertical diffusers carrying Gas-solid flow: experimental and numerical studies," *Powder Technology*, vol. 273, pp. 19-32, 2015.
- [22] J. S. Shuen, L. D. Chen and G. M. Faeth, "Evaluation of a stochastic model of particle dispersion in a turbulent round jet," *Am. Inst. Chem. Eng.*, vol. 29, p. 167-170., (1983).
- [23] M. Sommerfeld and N. Huber, "Experimental analysis and modeling of particle-wall collisions," *Int. J. Multiphase Flow*, vol. 25, p. 1457-1489., (1999).
- [24] E. Heintz and M. Bohnet, "Calculation of particle-wall adhesion in horizontal gas-solid flow using CFD," *Powder Technol.*, vol. 159, pp. 95-104, (2005).
- [25] M. Sommerfeld, "Modeling of particle-wall collisions in confined gas-particle flows," *Int. J. Multiphase Flow*, vol. 183, pp. 905-926, (1992).
- [26] B. Oesterle and A. Petitjean, "Simulation of particle-to-particle interactions in gas solid flows," *Int. J. Multiphase Flow*, vol. 19 (1), pp. 199-211, (1993).
- [27] C. Crowe, M. Sommerfeld and Y. Tsuji, "Multiphase Flow With Droplets and Particles," CRC Press, Florida, USA, 1998.
- [28] A. Eghlimi, A. Kouzoubov and C. A. J. Fletcher, "A New RNG-based two-equation model for predicting turbulent gas-particle flows," *International Conference on CFD in Mineral & Metal processing and power generation*, (1997).
- [29] W. A. El-Askary and A. Balabel, "Prediction of reattaching turbulent shear flow in asymmetric divergent channel using linear and non-linear turbulent models," *Eng. Res. J.*, vol. 30 (4), pp. 535-550, (2007).
- [30] W. A. El-Askary, I. M. Eldesoky, O. Saleh, S. M. El-Behery and A. S. Dawood, "Behavior of downward turbulent gas-solid flow through sudden expansion pipe," *Powder Technology*, vol. 291, pp. 351-365, 2016.

- [31] C. K. Chen, H. Q. Zhang and K. S. Lau,
"Numerical simulation of gas-particle flows
behind a backward-facing step using an
improved stochastic separated flow model,"
Computational mechanics, vol. 27(5), pp. 412-
417, 2001.